### by J. O. Dukovic

# Feature-scale simulation of resist-patterned electrodeposition

A numerical simulation of resist-patterned or "through-mask" electroplating has been performed to investigate shape evolution at the scale of small lithographic features. Shape evolution and step coverage have a significant influence on the shapes of such microelectronic structures as conductor lines. vias, and magnetic pole pieces. The simulation and associated analysis are based on a model for the rate distribution of the electrodeposition reaction that includes the depletion of the depositing metal ions and the inhibiting action of leveling agents. A stagnant boundary layer is assumed to be present, and the diffusion theory of leveling with a oneparameter description of kinetic inhibition is employed. The results show that when the geometry of a feature cavity makes possible the occurrence of concentration-field effects (such as radial diffusion), an uneven metal-ion flux should cause nonuniform growth at high fractions of the limiting current, and leveling agents should exert an opposing effect, even causing a strong reverse nonuniformity in some cases.

### Introduction

The use of patterned electrodeposition in electronic microfabrication is widespread and growing. Applications

include magnetic recording heads [1], masks for X-ray lithography [2], thin-film wiring on multichip packaging modules [3], bumps and solder balls for chip connection [4], and flexible packages [5]. One reason why electroplating has been achieving importance among methods for depositing thin metal films is the recent trend toward the use of copper in thin-film wiring structures [6]; copper plating is a relatively fast and inexpensive process. Of equal importance is the increased recognition of the extraordinary pattern-transfer capabilities of electroplating [7].

Typically, resist-patterned electrodeposition is carried out by the following steps:

- Deposit a thin conductive seed layer by evaporation or sputtering.
- Apply, expose, and develop the resist, leaving openings or cavities.
- Electrodeposit metal, which fills the cavities and replicates the resist pattern.
- 4. Strip the resist and remove the nonplated portions of the seed layer by etching.

The above procedure, often called "through-mask" plating, was pioneered by Romankiw and coworkers [8].

In most applications of through-mask plating, a flat profile is desired. For example, in thin-film wiring for packaging or device interconnection, one would like each conducting line to have the highest possible cross-sectional area without exceeding width or height ground rules. A flat

<sup>c</sup>Copyright 1993 by International Business Machines Corporation. Copying in printed form for private use is permitted without payment of royalty provided that (1) each reproduction is done without alteration and (2) the Journal reference and IBM copyright notice are included on the first page. The title and abstract, but no other portions, of this paper may be copied or distributed royalty free without further permission by computer-based and other information-service systems. Permission to republish any other portion of this paper must be obtained from the Editor.

profile (rather than a crowned or sunken one) best satisfies this preference. Furthermore, flatness may be necessary in fabricating multilayered structures by repeated patterned plating. Flatness is generally desirable in fabricating magnetic pole pieces for recording heads. Also, one usually expects bonding pads to have flat and regular surfaces. Bumps and solder balls used for chip joining may not require flat profiles, but their shapes should at least be uniform and regular. It can be reasoned that two nearby features of different sizes would be more likely to grow to the same height under conditions that would produce a flat rather than a humped or sunken profile.

In general, electronic components must be fabricated with high precision. Uniformity and yield must be extremely high for each manufacturing step in order for processes involving hundreds of steps to be economically viable. The corresponding need for quality and control in electronic microfabrication calls for clear knowledge of process behavior, parametric dependencies, safe operating windows, and process limits. Whether or not a flat profile is sought, most applications of electrodeposition in microelectronic fabrication call for high-precision, uniform, predictable behavior. The capability to predict feature shape evolution and the associated gain in understanding are of considerable potential value to those who design devices and fabrication processes.

A noteworthy numerical investigation of resist-patterned electrodeposition was conducted by Hume, Deen, and Brown [9]. This investigation, which was briefly reviewed by this author in [10], treated shape evolution in rectangular trench filling in a nonleveling system; the influences of metal-ion depletion and concentration-field effects were examined.

The investigation described here consisted of numerical simulations of profile evolution in through-mask electroplating. Its purpose was to learn how and to what extent such effects as metal-ion depletion and radially enhanced inhibitor transport can influence the ultimate shape of small structures fabricated by through-mask plating.

Behavior was studied in terms of departures from a central set of conditions, or "base case." This set of conditions was chosen to correspond to copper plating from an acid-sulfate bath into sparsely placed 10- $\mu$ m-wide cavities defined by a 5- $\mu$ m-thick resist layer. It was realized early that a more interesting and illustrative study would ensue if the base case were chosen so that the fraction of limiting current was higher than typically encountered in through-mask plating. Hence, we chose a rather high current density ( $50 \text{ mA/cm}^2$ ), low metal-ion concentration (100 millimolar), and thick boundary layer ( $40 \mu$ m). At more moderate values of the above three parameters, depletion of the metal ion plays an insignificant role, and, in the absence of leveling agents,

the resulting profiles would be extremely flat. (This important characteristic of through-mask plating is further discussed in the Conclusions section.) Finally, the resist wall was assumed to be vertical in the base case, and the inhibiting effect of the leveling agent was ignored. The base values of all the constants and dimensionless groups used are listed at the end of the paper.

### Theory and mathematical model

During the course of electrodeposition, the surface of the electrode gradually advances into the space previously occupied by the electrolyte. The rate of advance may vary with position, since the local rate of electrodeposition, usually proportional to the local current density, is dictated by electrochemical transport phenomena and electrode kinetics. The dominant mode of transport of the depositing ions and inhibitors at the 10-µm scale and below is diffusion. Highly nonuniform diffusive fluxes can arise from geometric concentration-field effects. Hence, the current distribution can be strongly affected by the geometry of the electrode surface and the surrounding resist structure. In turn, the electrode shape is gradually affected by the current distribution. The resulting shapeevolution behavior can be quite complicated. The final shape embodies the cumulative record of a succession of instantaneous reaction-rate distributions. Our aim was to simulate the shape evolution numerically by solving for the current distribution at each in a succession of time steps and using this solution to advance the boundary incrementally. We began by making a series of assumptions to express the problem in a manageable form.

### • Assumptions

The electrolyte was considered to be uniformly conductive despite the depletion of the depositing ions near the electrode surface. Under this assumption, valid for most plating baths (which contain excess supporting electrolyte), the potential obeys the Laplace equation.

We assumed that any departure from the bulk concentration of any species is confined to a concentration boundary layer near the electrode surface. We considered the outer edge of this layer to be flat, even though the resist-patterned electrode surface is topographic. We considered transport within the concentration boundary layer to be by diffusion alone; i.e., we assumed a stagnant diffusion layer. This common approximation greatly simplified the problem by obviating a detailed treatment of convection. Both the depositing metal ion species and the leveling agent were assumed to obey Fick's second law of diffusion within the concentration boundary layer. The instantaneous concentration fields were assumed to be pseudo-steady; this is a safe assumption, since the time scale for boundary motion greatly exceeds that for relaxation of the concentration field [11]. The outer edge of the diffusion layer was not considered to advance as the deposit grows; the error introduced by this assumption for the case treated, pertaining to films growing to a thickness one tenth that of the diffusion layer, is likely to be small.

Current efficiency was assumed to be 100 percent, which is nearly true for copper deposition but not universally true in electrodeposition.

We assumed that, in the absence of leveling, the kinetics of electrodeposition are dictated by the Butler-Volmer equation, with the exchange current density depending on reagent concentration as described by Newman [12]. We used the common expression for concentration overpotential given by Newman [13].

It was assumed that the widely recognized diffusion theory of leveling applies [14, 15]. According to this theory, the leveling agent is continuously consumed at the cathode surface. It is transported to the surface by convective diffusion; within the mass-transfer boundary layer, diffusion is the predominant mode of transport. While adsorbed to the surface, the leveler and/or its reaction products act to inhibit metal deposition. Since a higher surface concentration of inhibiting adsorbates is expected at points on the electrode that are exposed to a high diffusive flux of leveler, the rate of metal deposition is selectively suppressed at such points. Hence, as the electrode profile advances, protrusions tend to attenuate and cavities tend to fill.

The above mechanism is well accepted for many electroplating systems [14, 16]. Further, it has been proven that the leveling agent is consumed at its diffusion-limited rate in several systems of importance [17].

Dukovic and Tobias [11] have argued that the usual dependence of current density i on surface overpotential  $\eta_s$  for a nonleveling system,

$$i = i(\eta_s), \tag{1}$$

can be applied to a leveling system if modified to include only one more independent variable, the flux of the leveling agent  $N_{\rm A}$ , namely

$$i = i(\eta_s, N_A). (2)$$

This functional dependence is consistent with the rotatingdisk polarization data of Kruglikov et al. [18] for coumarin in a Watts nickel plating bath.

Jordan and Tobias [19] have shown that an even simpler relationship can be used. In a given system at a given overpotential, the current density is lower when the leveling agent is present than when it is absent by a factor that depends on the ratio of the leveling-agent flux to the metal-ion flux  $N_{\rm A}/N_{\rm M}$ , namely

$$i_{\text{levelling}}^{\text{ with}} = i_{\text{levelling}}^{\text{ without}} \frac{1}{1 + k_{\text{LEV}} \frac{N_{\text{A}}}{N_{\text{M}}}},$$
 (3)

where  $i_{\text{leveling}}^{\text{with}}$  and  $i_{\text{leveling}}^{\text{without}}$  are the current densities in the presence and absence of the leveling agent.\* This dependence was derived by Jordan and Tobias from an area-blockage treatment by Krichmar [20], which was later extended by Roha and Landau [21, 22]. Jordan and Tobias have shown that the above dependence produced a good fit to the polarization data of Kruglikov et al. [18] for the nickel-coumarin system.

Equation (3) permits a convenient separation of functional dependencies; the leveling effect can be described relative to the additive-free kinetic behavior, which is independent of the action of leveling additives:

$$i_{\text{leveling}}^{\text{ with }} \left( \frac{N_{\text{A}}}{N_{\text{M}}}, \, \eta_{\text{s}} \right) = f \left( \frac{N_{\text{A}}}{N_{\text{M}}} \right) i_{\text{leveling}}^{\text{ without }} (\eta_{\text{s}}).$$
 (4)

A further advantage of Equation (3) is that the function of  $N_{\rm A}/N_{\rm M}$  involves only one parameter,  $k_{\rm LEV}$ .

Although the above one-parameter description is certainly an oversimplification of real leveling systems, it does describe the essential behavior of leveling by a diffusion-limited inhibitor. Such a simple treatment is appropriate for the study undertaken. In future simulations involving specific systems or requiring high predictive power, more complicated or empirical functional dependencies can be substituted.

### • Mathematical model

Figure 1 shows the assumed geometry of the system and a concise statement of the mathematical model used. The model combines three different field problems in the potential  $\phi$ , the metal-ion concentration  $c_{\rm M}$ , and the leveling-agent concentration  $c_{\rm A}$ . In the figure, the superscript 'denotes the normal derivative. The three field problems are coupled at the electrode boundary only. The next three paragraphs describe the field problems.

The domain of the potential problem extends fully from the surface of the patterned electrode to a constant-flux boundary far away. The potential is assumed to obey the Laplace equation,

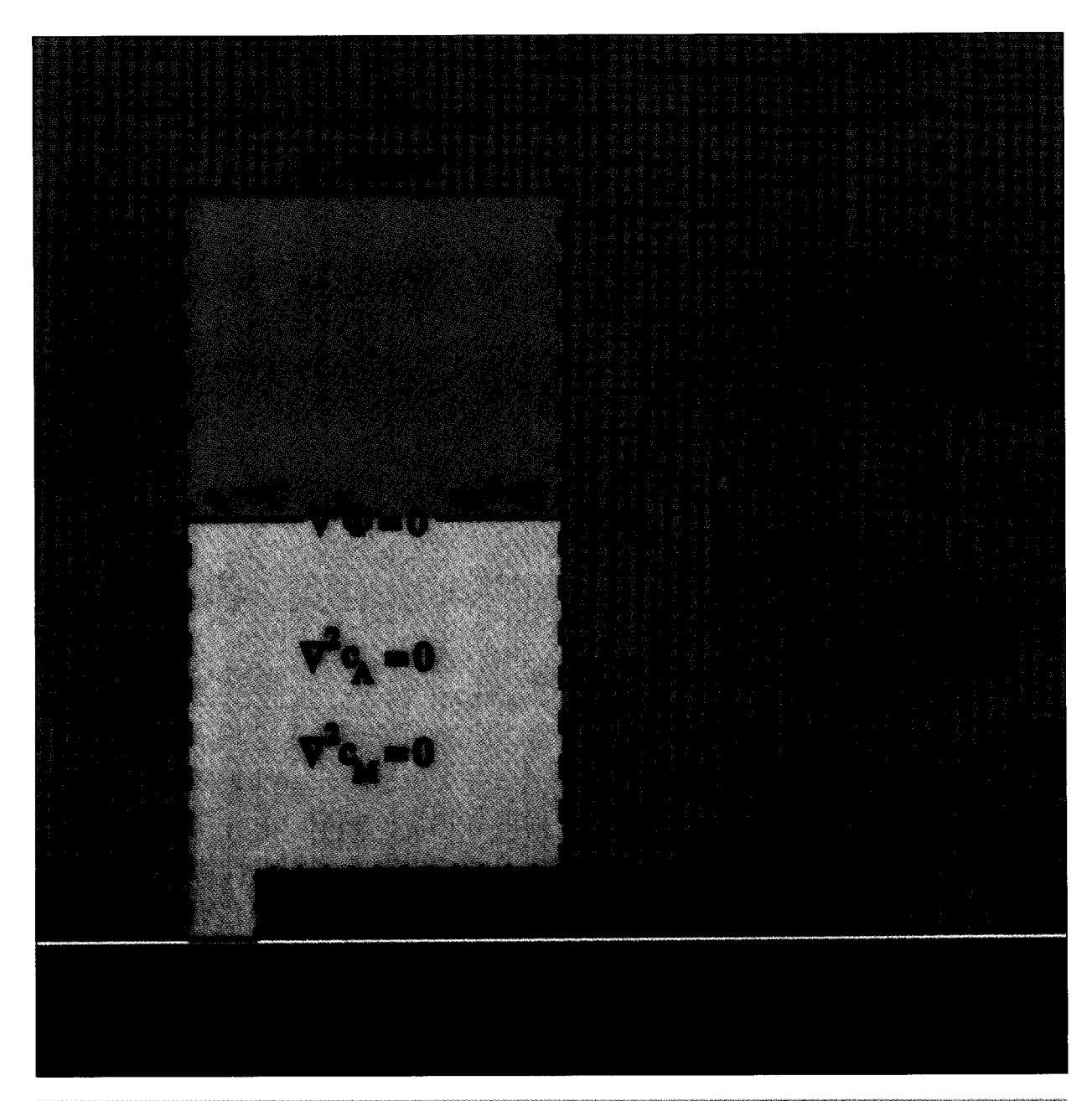
$$\nabla^2 \phi = 0. ag{5}$$

The current density is related to the potential by Ohm's law,  $i = -\kappa \nabla \phi$ . The boundary conditions on Equation (5) are as follows. The normal component of the potential gradient is assumed to be zero at all insulating and symmetry boundaries:

$$\nabla \phi \cdot \mathbf{n} = 0; \tag{6}$$

these boundaries include the resist surface, the symmetry axis that divides the feature in two, and the symmetry axis between adjacent features. At the boundary far away from

<sup>\*</sup>Nomenclature different from that used by Jordan and Tobias is used in this equation.



### FireIII as

The coupled boundary-value problem treated in this paper [Equations (5)–(15) and (23); some equations are abbreviated] and the geometric configuration of the problem. Concentration domain — light-blue region; potential domain — pink and light-blue regions; photoresist — red region; substrate — lavender region; seed layer for electrodeposition — yellow strip. Geometric parameters are indicated in purple.

the electrode surface, the normal derivative of potential is set to a constant value. This value is chosen to be that necessary to supply an average current density of  $\overline{i}$  to the exposed surface of the cathode at time zero. The total currents at the cavity and at the far boundary are forced to balance by the boundary value problem; the current

densities differ, however, according to the ratio of surface areas, w/p. Thus,

$$\nabla \phi \cdot \mathbf{n} = -\frac{\overline{i}w}{\kappa p}. \tag{7}$$

At the electrode surface, the potential obeys an equation

128

relating its normal derivative (which is proportional to the reaction rate) to the potential difference acting across the electrode surface (the driving force for electrodeposition). The potential of the electrode itself is arbitrarily taken to be zero; hence the value of potential within the electrolyte at the electrode surface represents the negative of the total overpotential,  $\phi = -\eta_{\rm tot}$ . The relation between reaction rate and potential difference is stated below as Equation (23); since this involves the other two field variables  $c_{\rm M}$  and  $c_{\rm A}$ , it is described later. Also at the electrode surface, the normal derivative of potential is related to the normal derivative of metal-ion concentration by the flux-matching condition [Equation (11)] described below.

The concentration of metal ions varies within a smaller domain, that of the concentration boundary layer. Within this domain, Fick's second law results in the Laplace equation:

$$\nabla^2 c_{\mathsf{M}} = 0. \tag{8}$$

Again, there is no normal gradient (no flux) at the resist surface or at either symmetry boundary. Thus,

$$\nabla c_{i,i} \cdot \mathbf{n} = 0. \tag{9}$$

At the outer edge of the boundary layer, the metal-ion concentration is assumed to be held at its bulk value:

$$c_{\mathsf{M}} = c_{\mathsf{M}}^{\,\circ} \,. \tag{10}$$

At the electrode surface, the normal derivatives of  $c_{\rm M}$  and  $\phi$  are proportional, since the flow of current is entirely due to electrochemical reaction of the metal ions, which are transported only by diffusion. Thus,

$$nFD_{\mathbf{M}}\nabla c_{\mathbf{M}} \cdot \mathbf{n} = \kappa \nabla \phi \cdot \mathbf{n}. \tag{11}$$

The third field problem involves the leveling agent, whose concentration again varies only within a diffusion boundary layer. (The two boundary layers are assumed for simplicity to have the same thickness, although this may not be strictly true.) In this domain, the Laplace equation applies once again:

$$\nabla^2 c_{_{\mathbf{A}}} = 0. \tag{12}$$

Again, no flux is allowed across any insulating or symmetry boundary:

$$\nabla c_{\mathbf{A}} \cdot \mathbf{n} = 0. \tag{13}$$

As for the metal ions, the leveling-agent concentration is set to its bulk value at the outer edge of the boundary layer:

$$c_{\rm A} = c_{\rm A}^{\alpha} \,. \tag{14}$$

Since the leveling agent is being consumed at its transportlimited rate, its concentration is zero at the electrode surface:

$$c_{A} = 0. ag{15}$$

The leveling-agent field problem can be solved independently of the metal-ion and potential problems. However, the overpotential expression contains the leveling-agent flux, as was described in the previous section.

There are two boundary conditions at the electrode surface that link the three field problems together. The first is Equation (11), which equates the ohmic and diffusive expressions for the electrode current. The second is the overpotential expression, which is rather complicated because it includes surface overpotential, concentration overpotential, and the dependence of the rate constant on both metal-ion concentration and leveling-agent flux. This equation, the rate expression for electrodeposition, is derived in the following paragraph.

The potential of the electrolyte at the electrode surface  $\phi$  is related to the total overpotential  $\eta_{\text{tot}}$  by an arbitrary additive constant  $\phi_{\text{E}}$ :

$$\phi = \phi_{\rm E} - \eta_{\rm tot} \,. \tag{16}$$

Setting  $\phi_{\rm E}$  equal to zero and resolving the overpotential into its two components yields

$$\phi = -\eta_s - \eta_c, \tag{17}$$

where  $\eta_{\rm s}$  is the surface overpotential and  $\eta_{\rm c}$  is the concentration overpotential. The concentration overpotential arises because the metal-ion concentration near the electrode surface  $c_{\rm M}$  differs from the bulk concentration  $c_{\rm M}^{\infty}$ :

$$\eta_{c} = \frac{RT}{nF} \ln \frac{c_{M}}{c_{M}^{\infty}}.$$
 (18)

The surface overpotential  $\eta_s$ , associated with the activation energy of the electrode reaction, is related to the current density *i*. The present analysis is based on the widely used Butler-Volmer equation of electrode kinetics,

$$i = i_0 \left[ e^{\alpha_0} \frac{\eta_s F}{RT} - e^{-\alpha_0} \frac{\eta_s F}{RT} \right]. \tag{19}$$

The exchange current density  $i_0$  is assumed to depend on the metal-ion concentration, as described by Newman [12]:

$$i_0 = i_0^{\infty} \left(\frac{c_{\rm M}}{c_{\rm M}^{\infty}}\right)^{\gamma}. \tag{20}$$

Further, the exchange current density is assumed to depend on the leveling-agent flux according to Equation (3), namely

$$i_0^{\infty} = i_0^{\infty, c_A = 0} \left( \frac{1}{1 + k_{\text{LEV}} \frac{N_A}{N_M}} \right).$$
 (21)

129

The last equation can be rephrased by expressing the metal-ion flux in terms of current density,  $N_{\rm M} = i/nF$ :

$$i_0^{\infty} = i_0^{\infty, c_A = 0} \left( \frac{1}{1 + k_{\text{LEV}} nF \frac{N_A}{i}} \right).$$
 (22)

Finally, substitution of Equations (17), (18), (20), and (22) into Equation (19) produces the overpotential boundary condition, which relates the values of i,  $\phi$ ,  $c_{\rm M}$ , and  $N_{\rm A}$  at the electrode surface:

$$i = i_0^{\infty, c_A = 0} \left( \frac{1}{1 + k_{\text{LEV}} nF \frac{N_A}{i}} \right) \left( \frac{c_M}{c_M^{\infty}} \right)^{\gamma}$$

$$\cdot \left\{ \exp \left[ -\alpha_a \left( \frac{\phi F}{RT} + \frac{1}{n} \ln \frac{c_M}{c_M^{\infty}} \right) \right] - \exp \left[ \alpha_c \left( \frac{\phi F}{RT} + \frac{1}{n} \ln \frac{c_M}{c_M^{\infty}} \right) \right] \right\}. \tag{23}$$

### • Dimensionless problem statement

The three-way coupled field problem stated above is made dimensionless according to the following scheme. Lengths are made relative to the feature width w. Concentrations are referred to their bulk values. Current densities are nondimensionalized with respect to the average current density at the initial feature surface  $\bar{i}$ . Potentials are related to the quantity  $\bar{i}w/\kappa$ . The fluxes of metal ion and leveling agent are divided by  $D_{\rm M}c_{\rm M}/w$  and  $D_{\rm A}c_{\rm A}/w$ , respectively. The resulting set of dimensionless equations follows. (Asterisks are used to signify dimensionless quantities and operators.)

Within the electrolyte,

$$\nabla^{*2} \phi^* = 0. \tag{24}$$

Far away from the cathode,

$$\nabla^* \phi^* \cdot \mathbf{n} = w/p. \tag{25}$$

Within the concentration boundary layer,

$$\nabla^*{}^2c_{\mathbf{M}}^*=0$$

and

$$\nabla^*{}^2c^* = 0.$$

At the outer edge of the boundary layer,

$$c_{M}^{*} = 1$$

and

$$c_{\Lambda}^* = 1.$$

130 At the resist surface and symmetry boundaries,

$$\nabla^* \phi^* \cdot \mathbf{n}^* = 0, \tag{30}$$

$$\nabla^* c_{\Lambda}^* \cdot \mathbf{n}^* = 0, \tag{31}$$

and

$$\nabla^* c_{\scriptscriptstyle M}^* \cdot \mathbf{n}^* = 0. \tag{32}$$

At the cathode surface,

$$c_{\Lambda}^* = 0, \tag{33}$$

$$\nabla^* c_{\scriptscriptstyle M}^* \cdot \mathbf{n}^* = Sh \, \nabla^* \phi^* \cdot \mathbf{n}^*, \tag{34}$$

and

$$\frac{Wa_{\rm T}}{Wa_{\rm L}} \left( 1 + \frac{\alpha_{\rm a}}{\alpha_{\rm c}} \right) \left( 1 + K_{\rm LEV} \frac{N_{\rm A}^*}{i^*} \right) \frac{1}{c_{\rm M}^{*\gamma}} i^*$$

$$= \exp\left( \frac{\phi^*}{Wa_{\rm T}} + \frac{\alpha_{\rm c}}{n} \ln c_{\rm M}^* \right)$$

$$- \exp\left[ -\frac{\alpha_{\rm a}}{\alpha_{\rm c}} \left( \frac{\phi^*}{Wa_{\rm T}} + \frac{\alpha_{\rm c}}{n} \ln c_{\rm M}^* \right) \right]. \tag{35}$$

The above set of equations contains seven independent dimensionless groups. Three of these involve only kinetic parameters that were already dimensionless:  $\alpha_a/\alpha_c$ ,  $\alpha_c/n$ , and  $\gamma$ . The other four groups are referred to by special names. Two are forms of the Wagner number [10]: the Tafel form,

$$Wa_{\mathsf{T}} = \frac{RT\kappa}{\alpha \, F\bar{i}w} \,, \tag{36}$$

and the linear form,

$$Wa_{L} = \frac{RT\kappa}{(\alpha_{c} + \alpha_{s})Fi_{0,c=0}^{\infty}W}.$$
(37)

Another group can be considered a Sherwood number,

$$Sh = \frac{\overline{i}w}{nFD_{\rm M}c_{\rm M}^{*}}.$$
 (38)

Finally, the dimensionless leveling parameter is defined as

(26) 
$$K_{\text{LEV}} = \frac{nFc_{\text{A}}^{\alpha}D_{\text{A}}}{\bar{i}w} k_{\text{LEV}}.$$
 (39)

### (27) Method of solution

(28)

(29)

The advancement of the electrode profile over time was treated stepwise via a succession of time intervals. At each interval, the above system of equations was solved for the corresponding profile geometry using an iterative numerical scheme. The resulting distribution of current at the electrode surface was used to advance the boundary in compliance with Faraday's law.

### • Iterative scheme

The starting point at each time interval was to solve the field equation for the leveling-agent concentration assuming an initially uniform current density. A profile of metal-ion concentration derivatives was then calculated using Equation (11) (flux matching). By using the latter profile as a boundary condition, the Laplace equation was solved. The resulting surface-concentration profile was substituted into the overpotential expression [Equation (23)] along with the leveling-agent flux profile. By using the most recent current-density profile, an overpotential profile was calculated. Next, these surface potentials were used as a boundary condition to solve the Laplace equation for potential. A new current-density profile was thereby calculated. A residual, consisting of the difference between the new and old current-density profiles, was evaluated. The multivariate Newton-Raphson method was used with this residual to obtain a better estimate of the currentdensity profile. The cycle was repeated until the largest relative change in current density at any point on the profile was smaller than 10<sup>-6</sup>. In most cases no more than five iterations were required for convergence. The boundary-element method with quadratic elements [23] was used to solve the individual field equations, as in an earlier work [24].

### • Moving-boundary algorithm

The method used for moving the boundary was similar to one previously reported [11], with one major difference: It was necessary in the present work to treat growth along an insulating wall. This is not straightforward when the wall is not vertical. Furthermore, since the side wall goes from being entirely bare to being mostly covered with metal, the number of nodes used to represent this boundary must be changed over the course of the simulation in order to prevent extreme local differences in element size. To this end, a scheme was devised for distributing nodes along the resist wall that roughly preserves their original spacing by letting the number of nodes on the segment decrease over time. A similar node redistribution scheme was used on the segment of the boundary describing the electrode surface. In this case, the number of nodes could increase or decrease depending on whether the exposed area was increasing or decreasing.

The following approach to growth along the resist wall was taken. We refer to the node at the intersection of the electrode profile and the resist wall as the "two-phase" node. After the preliminary relocation of the nodes according to Faraday's law, a test was conducted to see whether the two-phase node had been relocated within the resist (i.e., beyond the region where metal deposition is allowed). If so, a new quadratic element was formed along with the two nearest false electrode nodes, and the intersection of this false element with the resist wall was

located by marching along the element and testing at each point. The two-phase node was then relocated to this intersection point. If the two-phase node had been originally relocated within the cavity but off the resist wall, it was relocated to a point equidistant from its origin but lying on the resist wall. With these exceptions, the false surface was constructed and measured exactly as in [11]. Next, the number of elements to be used in the boundary-element representation of the new profile and their arc lengths were determined, using an algorithm that preserves both the relative lengths and the approximate absolute lengths of the elements. Finally, the nodes were repositioned on the false surface, as in [11]. No artificial smoothing of the profiles was performed.

In the base-case problem (described below), 76 nodes were used to describe the potential domain; 74 nodes described the concentration domains. Both numbers decreased as the simulation proceeded.

During each time interval, the volume of the deposit grows by the same increment. This growth increment was defined so that, in the case of unidirectional even growth, the profile would advance by one percent of the feature width w in each time step.

### Scheme of investigation

As already indicated, behavior was studied in terms of departures from a central set of conditions, or "base case." At the base case, the seven dimensionless groups were assumed to have the following base values: Sh = 0.5,  $K_{\text{LEV}} = 0$ ,  $Wa_{\text{T}} = 520$ ,  $Wa_{\text{L}} = 6500$ ,  $\alpha_{\text{a}}/\alpha_{\text{c}} = 3$ ,  $\gamma = 0.6$ , and  $\alpha_{\text{c}}/n = 0.25$ . The five geometric parameters were assumed to have the following base values: h/w = 0.5,  $\theta = 90^{\circ}$ ,  $\delta/w = 4$ , p/w = 10, and s/w = 50. The base case corresponds to (but is not restricted to) copper plating at 50 mA/cm<sup>2</sup> from a 100-mM-Cu<sup>2+</sup> bath with a 40- $\mu$ m-thick diffusion boundary layer into a 10- $\mu$ m-wide cavity with vertical walls.

In the parametric investigation, the following parameters were varied: current density  $(\bar{i}, \text{ reflected in } Sh \text{ and } Wa_T)$ ; boundary-layer thickness  $(\delta/w)$ ; resist thickness (h/w); wall angle  $(\theta)$ ; and leveling parameter  $(K_{\text{LEV}})$ . Also, a comparison was made of the growth in a cylindrical cavity and a semi-infinite trench.

It should be noted that the current flowing to the cavity (rather than the current density) was fixed throughout each simulation. This was done by fixing the current density at a boundary far away from the electrode,  $i_{\rm far}$ , namely,

$$i_{\text{far}} = -\frac{w}{p}\bar{i},\tag{40}$$

where  $\overline{i}$  refers to the average *initial* current density at the feature surface. As growth proceeds, the electroactive area of the feature usually changes; in such cases, the actual

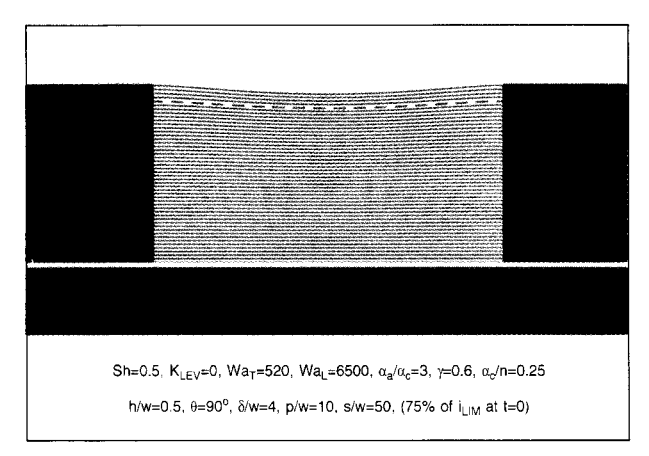


### Figure 2 Shape evolution predicted for the base case.

instantaneous average current density at the feature surface varies in inverse proportion to the electroactive area.

We have chosen to characterize the extent of deposition in terms of the mean height  $\bar{y}$  of the profile of the deposit. (More strictly, we refer to  $\bar{y}^* = \bar{y}/w$ , since all lengths were made dimensionless with respect to the feature width w.) The mean was calculated as follows: the height of a flat-profiled deposit of equal volume to the deposit in question.

The nonuniformity or departure from flatness of the profile of a deposit can be expressed as follows:

$$N = \frac{y_{\text{outer}} - y_{\text{center}}}{\bar{y}},\tag{41}$$

where  $y_{\text{center}}$  is the height of the deposit at the center and  $y_{\text{outer}}$  is defined as the opposite extreme in profile height, an extreme which does not necessarily occur at the very edge of the profile (as in the 70°-wall case discussed later). As defined, the magnitude of N reflects the degree of nonuniformity, and its sign indicates whether the profile is higher at the center (negative) or at the sides (positive).

It was necessary to choose a rational basis for comparing the nonuniformities in different cases. We compare values of N at the same value of  $\bar{y}/w$ . Specifically, we define  $N_{90}$  as the value of N when the mean thickness  $\bar{y}/w$  of the deposit reaches 90 percent of the resist thickness h/w.

It should be noted that the analysis was limited to growth within the resist walls. Each simulation was halted just before growth would have extended over the top of the resist layer ("overgrowth" or "mushrooming"). However, the resulting final profile for each case generally

corresponded to a different mean profile height  $\bar{y}/w$ , since the shape of each profile was different. The most meaningful comparison of nonuniformity from case to case was to compare the values of  $N_{\rm so}$ .

The fraction of the limiting current, which can be expressed as  $\overline{i}/\overline{l}_L$ , is a well-known parameter of importance in determining the impact of transport nonuniformities on current distribution. It may therefore appear desirable to attempt direct comparisons between different cases at the same fraction of limiting current. However, this is not practical for two reasons. First, the limiting current does not remain constant as the profile advances, since the problem geometry is not constant. Second, even the limiting current at time zero cannot be known a priori; it must be computed numerically for each problem geometry. Matching the initial limiting currents between two problems of different geometry would require at least one other parameter of the model to be set to unequal values. Such a procedure would be somewhat arbitrary and would require another level of iteration in the problem. In view of the above arguments, it was decided, for this work, to conduct a straightforward analysis based on the geometric parameters and dimensionless groups and to report the initial fraction of limiting current parenthetically.

### **Results and discussion**

The results of the analysis are presented in two types of plots. "Shape history plots," such as Figure 2, show a series of electrode profiles as light-blue curves. The resist is shown in red, the substrate in dark blue, and the conductive seed layer in vellow. The height and width dimensions are shown in true proportion. Each growth step corresponds to a fixed increment in electrode volume or in time, since the total current to the feature was held constant during each simulation. The profile corresponding to a mean deposit height that is approximately 90 percent of the resist height is highlighted as a dashed purple curve. Beneath each plot, the values of the seven dimensionless physico-chemical parameters are indicated on one line, and the values of the five geometric parameters are indicated on the next line (along with the initial fraction of the limiting current in parentheses). The parameters that depart from the base-case values are highlighted in red.

The other type of plot, for example that of **Figure 3**, shows the relative nonuniformity in the profile height N as a function of the average height  $\bar{y}$  to which the profile has grown. Such "nonuniformity plots" compare several different cases. Each curve is labeled with the number of the figure in which the shape history is shown. For example, Curve 2 in any nonuniformity plot corresponds to Figure 2 (the base case). A dashed vertical line corresponds to 90 percent of the resist wall height; the value of  $N_{90}$  can be read from the intercept of a curve with this line.

One other result is reported for each case in the discussion that follows: the fraction of the limiting current density at time zero,  $\overline{i}/\overline{i}_{\rm L}$ . It was calculated from the solution of the coupled boundary-value problem for the first time interval. The limiting flux of metal ions was not calculated directly; instead, it was determined from the identity between the dimensionless  $c_{\rm M}^*$  and  $c_{\rm A}^*$  fields, leading to the expression

$$\frac{\overline{i}}{\overline{i}_{L}} = \frac{\int_{x=0}^{x=\frac{w}{2}} \frac{\partial c_{M}^{*}}{\partial y^{*}} dx}{\int_{x=0}^{x=\frac{w}{2}} \frac{\partial c_{A}^{*}}{\partial y^{*}} dx}.$$
(42)

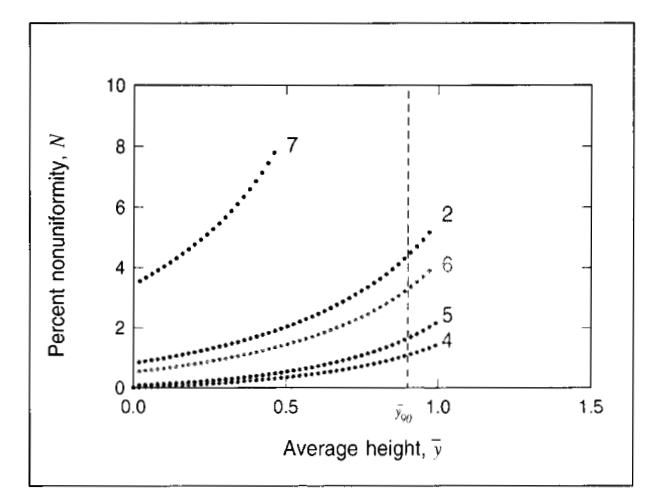
The integrals were evaluated numerically using the boundary-element interpolation functions. The value for  $\overline{i/l_L}$  is indicated in parentheses for each shape-history plot. It should be emphasized that this value was not treated as an independent variable in the system. Rather, the value of  $\overline{i/l_L}$  was uniquely determined by the seven dimensionless variables and five geometric parameters described earlier.

### Base case

Figure 2 shows the shape evolution predicted for the base case described in the previous section. As can be seen from the figure, the growth-rate distribution is fairly uniform throughout the time of deposition. Growth is slightly faster near the resist walls, especially as the deposit thickness approaches the resist thickness. When the profile has grown to an average height that is 90 percent of the resist height, the sides of the deposit are 4.5 percent higher than the center (i.e.,  $N_{90} = 4.5\%$ ). The evolution of profile nonuniformity is shown as Curve 2 in Figure 3. It is apparent from both Figures 2 and 3 that the nonuniformity arises primarily toward the end of the growth period. This occurs because the resist walls exert less of a collimating effect on the diffusive flux as the cavity fills, and radially enhanced diffusion causes slightly higher current density toward the walls. This trend was pointed out by Hume, Deen, and Brown [9].

### ■ Half current density

This case and all remaining cases studied were simple departures, usually of only one parameter, from the base case. Figure 4 shows the shape history that results when the deposit is grown at half of the base current density (half of the base deposition rate). This plating rate corresponds to 38 percent of the diffusion-limited current. The resulting nonuniformity, which is also reflected by Curve 4 in Figure 3, is quite mild:  $N_{90}=1.3\%$ . This illustrates that at a low or modest fraction of the limiting current, there is little basis for nonuniformity caused by uneven depletion of the depositing ions. This is because the component of overpotential due to the departure from



### F(0)1172

Predicted relative nonuniformity as a function of the height of the electrodeposited film. Curve numbers correspond to figure numbers. For the cases covered here, it is assumed that the wall angle is 90° and that there is no leveling. Nonuniformity for growth under the conditions of the base case (curve 2); for growth at half the base current density (curve 4); for growth in a round cavity (curve 5); for growth under strong agitation (curve 6); and for growth at half the base photoresist thickness (curve 7).

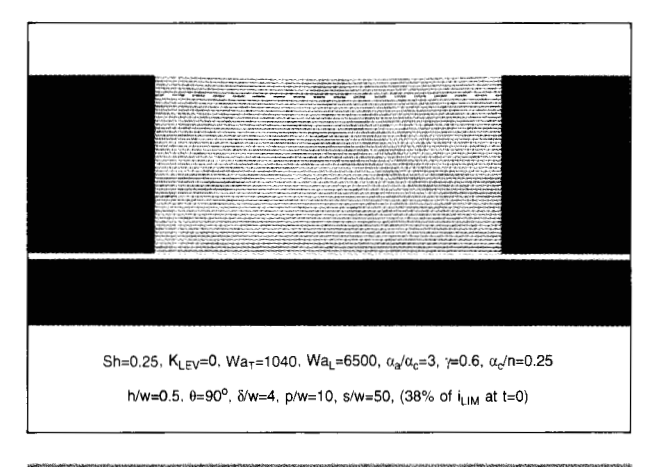


### Figure 4

Shape evolution predicted at half the base current density (base conditions otherwise).

bulk concentration is so small in *absolute* terms that no appreciable *relative* differences can arise to cause nonuniform deposition.

### • Round cavity (rather than trench)

A simulation performed for the case of a round cavity of diameter equal to the width of the trench in the base case

133

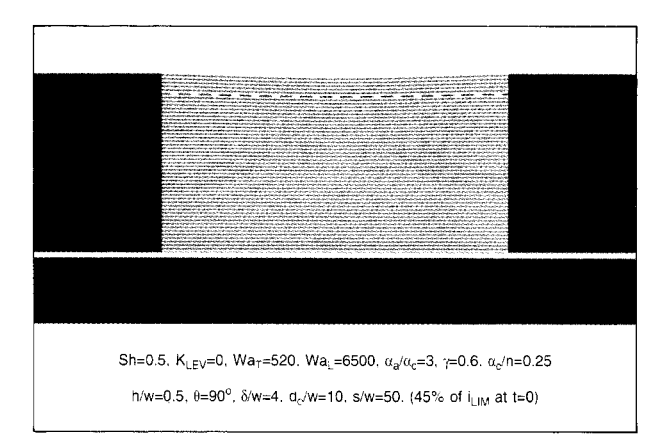


### Figure 5

Shape evolution predicted for a round cavity (axisymmetric problem) rather than a semi-infinite trench (base conditions otherwise).

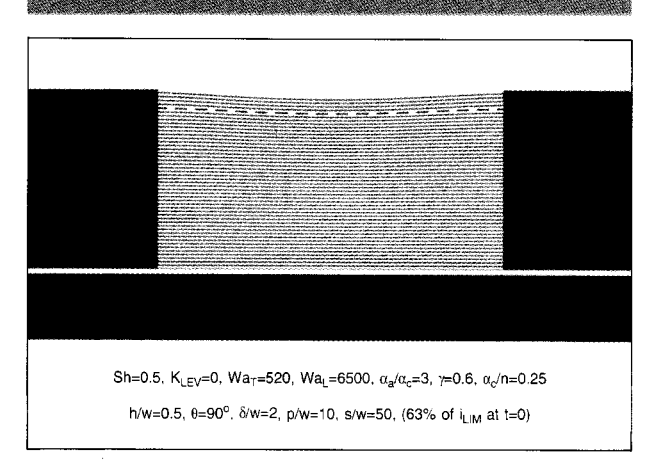


### Figure 6

Shape evolution predicted at half the base value of the diffusionlayer thickness (base conditions otherwise).

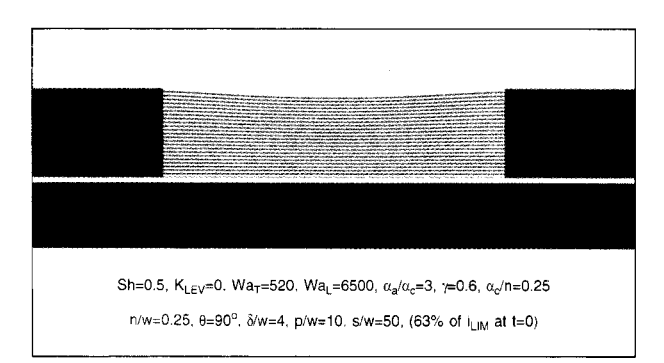


### Figure 7

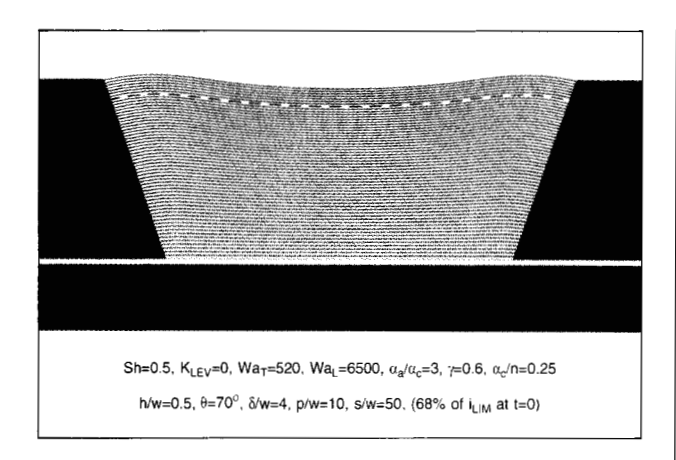
Shape evolution predicted at half the base resist thickness (base conditions otherwise).

produced the shape history in Figure 5. This is the only case in which the problem was treated in cylindrical rather than Cartesian coordinates. The domain was bounded by a cylindrical no-flux boundary of diameter  $d_0$  equal to the interfeature spacing p used in all the other cases studied. It should be recognized that this case is special because spherical diffusion is well known to be stronger than radial (i.e., cylindrical) diffusion. Consequently, the limiting current to a round cavity should be high; this case involves a lower fraction of the initial limiting current (45%) than for the base case (75%). As a result, mild uniformities should be expected from the argument given above for the case of half current density. One is therefore not surprised to find that the nonuniformity is significantly less than in the base case,  $N_{90} = 1.8\%$ . (Figure 3 permits a clear comparison.) Again, this difference exists because spherical diffusion is stronger than radial diffusion. At a lower overall fraction of the limiting current, spatial nonuniformity in mass transfer accessibility has less impact. This effect actually defeats the tendency for the round cavity to attract more diffusive flux to its walls than would a trench.

• Strong agitation (half boundary-layer thickness) The shape history resulting from halving the diffusion-boundary-layer thickness is shown in **Figure 6**. The uniformity improves, as is evident from Figure 3;  $N_{90}$  decreases from 4.5 to 3.5 percent. The main cause of this improvement is that the fraction of the limiting current has decreased from 75% to 63%. Again, differences in metalion depletion from point to point can only cause nonuniform growth to the extent that the overall level of depletion is high.

### • Half resist thickness

The simulation of growth confined by a resist layer half as thick as in the base case resulted in the shape history of Figure 7. The evolution of the relative nonuniformity is shown in Curve 7 of Figure 3. Although the absolute difference in height from side to center (as a percentage of w, for example) is less than in the base case, the difference relative to mean height is significantly greater; i.e.,  $N_{90}$  is 7.6% for the thin resist, compared to 4.5% for the base case. It is more meaningful to compare two profiles of the same average height, most appropriately 90 percent of the thinner resist. While N is 7.6% at this point for the thin resist, N is only 2.0% at the same point in time for the fullthickness resist. This can be explained as follows: In a shallow cavity, the cavity walls exert less of a collimating effect on diffusive flux. Thus, the radial enhancement is higher than for a deep cavity. Hume, Deen, and Brown [9] have referred to this effect. This result suggests that one strategy for achieving nearly flat profiles is to use a resist somewhat thicker than the intended thickness of the deposit.





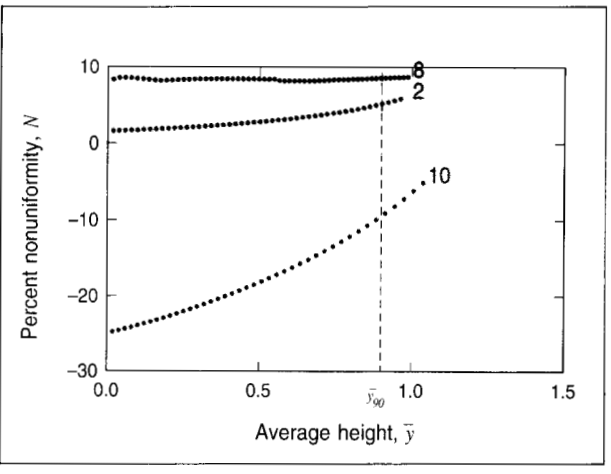
Shape evolution predicted at base conditions and a wall angle of  $70^{\circ}$ .

### Wall angle of 70°

The cases discussed so far have pertained to vertical resist walls ( $\theta = 90^{\circ}$ ). In Figure 8, the predicted growth history at a 70° wall angle is shown. Curve 8 in Figure 9 indicates nonuniformity at all profile heights. It should be remembered that the total current to the cavity is held constant over time; hence, the rate of advance declines gradually as the profile widens. The resulting profile has an interesting shape. The lowest point on the profile is the center, and the highest points are not at the walls but slightly inward from them. The informal expression "rabbit ears" is sometimes used to refer to this type of profile, especially when inspected by profilometry, which exaggerates the vertical dimension. This shape results from the increased accessibility of the sides by the diffusing metal ions, because of the obtuse angle formed by the resist wall and the surface of the deposit. In this case,  $N_{90}$  is 7.8%.

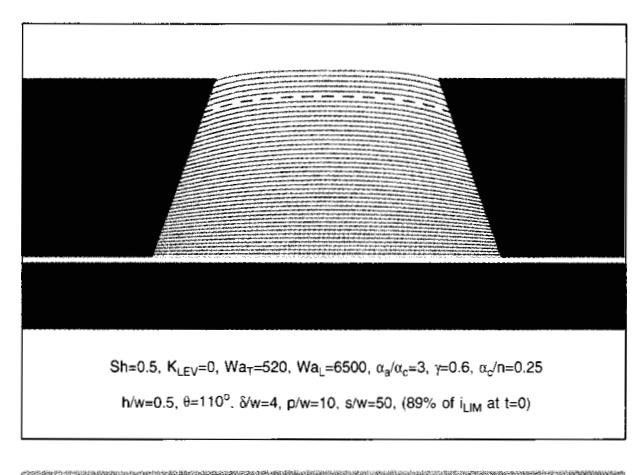
### Wall angle of 110°

Figure 10 shows a simulation for a reentrant cavity. At each time step, the electroactive area is smaller; hence, the rate of advance increases over time. It takes significantly less time and less metal to fill such a cavity than the one described above. The resulting profile is highest at the center and has a "crowned" or mounded shape. The acute angle between resist wall and the electroactive surface causes increased local depletion of metal ions at the walls (as a result of the field nature of diffusion). Also, the limiting current is lower for this narrow cavity than for lower wall angles. The initial fraction of limiting current is 89 percent. For this case,  $N_{90}$  is -9.5%. The nonuniformity is plotted as Curve 10 in Figure 9; N, by



### Tile (IIIG)

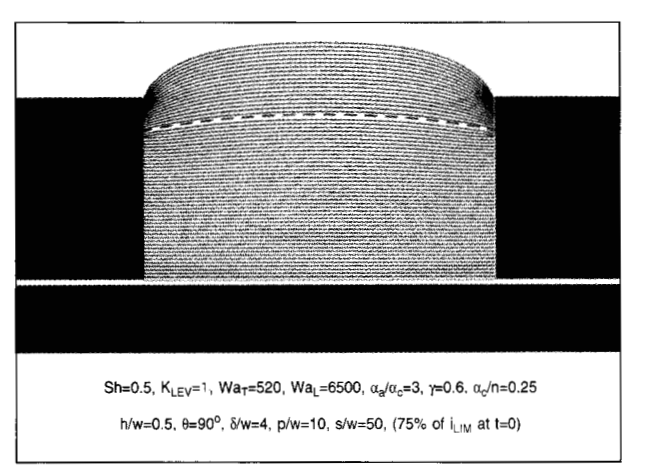
Predicted relative nonuniformity as a function of the height of the deposited film at wall angles of 90° (curve 2), 70° (curve 8), 110° (curve 10); base conditions otherwise.



### Figure 10

Shape evolution predicted at a wall angle of  $110^{\circ}$  (base conditions otherwise).

definition, has a negative value for a crowned profile. Toward the beginning of growth, N is large and negative for two reasons: The fraction of limiting current is very high (89%), and the wall angle causes a strong field effect, leading to severe depletion in the corners. As the cavity fills, the fraction of limiting current rises, and there is increased transport at the walls by radial diffusion; both factors cause the magnitude of nonuniformity to decrease. Figure 9 compares three cases that differ only in wall angle.



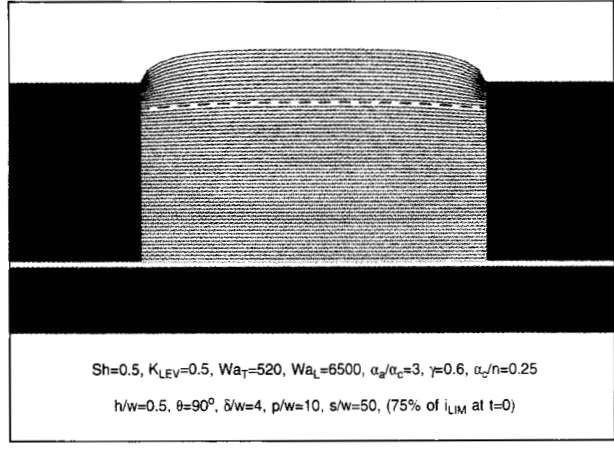


### Figure 11

Shape evolution predicted under strong leveling ( $K_{\rm LEV}=1$ , base conditions otherwise).

### Figure 13

Shape evolution predicted under moderate leveling ( $K_{\rm LEV}=0.5$ , base conditions otherwise).

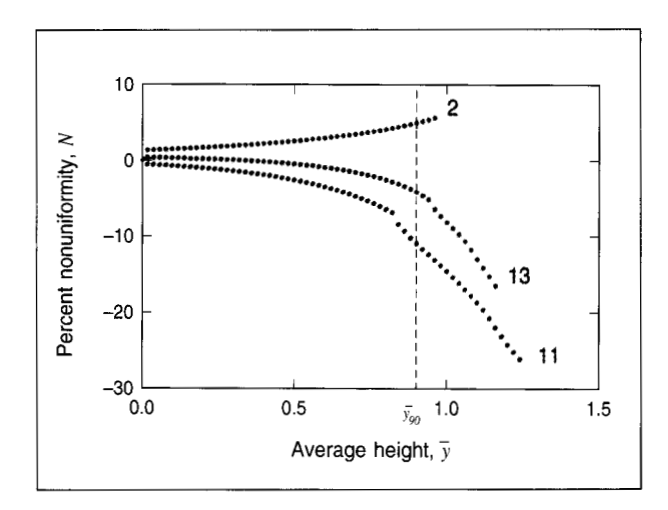


### Figure 12

Predicted relative nonuniformity as a function of the height of the deposited film at three different values of the leveling parameter:  $K_{\rm LEV}=0$  (curve 2);  $K_{\rm LEV}=0.5$  (curve 13);  $K_{\rm LEV}=1$  (curve 11); base conditions otherwise.

## Electrodeposition is preferentially inhibited at the sides, where transport of the leveling agent is radially enhanced. In this case, $N_{90}$ is -10.9%. It is interesting to note that the rate of advance along the resist wall decelerates greatly near the top of the cavity. This is because there is higher geometric accessibility by diffusion as the profile advances.

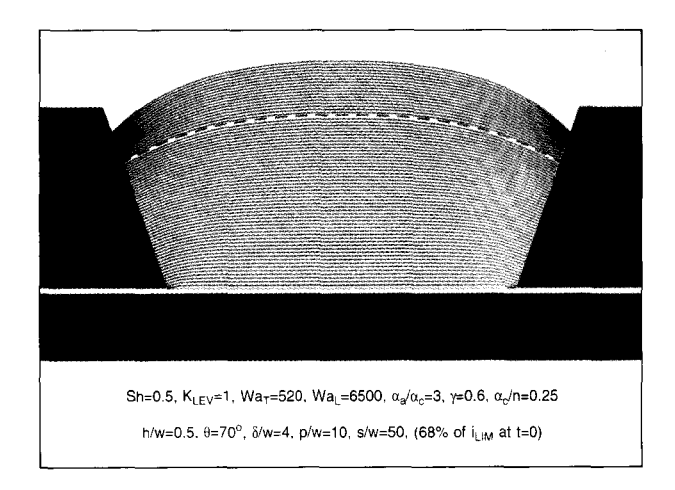
It is worth mentioning that, although it is diffusion that causes both the antileveling and leveling effects, there are some key differences in the two effects. First, the leveling agent is assumed to be entirely diffusion-controlled, a condition at which severe geometric enhancements can result (even infinite in magnitude for certain geometric cases, although kinetic influence would prevent this); the metal ions cannot deposit at their diffusion limit without ruining the quality of the deposit. Second, the rate expression involves only the gradient of the leveling-agent concentration, while it primarily involves the concentration of the metal ions.

### Strong leveling

In the simulations described so far, the leveling parameter was set to zero. Figure 11 shows the result of plating at base conditions but with  $K_{\rm LEV}$  set to 1.0. There is a dramatic reversal in the shape history from the case of no leveling. The deposit is crowned, i.e., is highest at the center and lowest at the two sides. The associated nonuniformity is shown as Curve 11 of Figure 12.

### Moderate leveling

Figure 13 shows that when the leveling parameter is set to 0.5 rather than 1, the crowning effect is reduced significantly; in this case,  $N_{90}$  changes from -10.9% to -4.4%. (Compare Curves 11 and 13 in Figure 12.) Very roughly, one could say that the effect is nearly linear (bearing in mind that  $N_{90}$  is +4.5% when  $K_{\rm LEV}=0$ ). Figure 12 compares two cases with leveling (Curves 11 and 13) to the base case (Curve 2). The slight discontinuity in Curves 11 and 13 is most likely a numerical artifact associated with the discrete representation of the boundary and the





Shape evolution predicted under strong leveling and a 70° wall angle ( $K_{\rm LEV}=1, \ \theta=70^{\circ}$ , base conditions otherwise.)

extreme variation of leveling-agent flux with profile-to-wall angle in the vicinity of 90°.

### • Strong leveling, 70° wall angle

The impact of the leveling agent is quite prominent when the wall angle is such that radial enhancement to the sides is important throughout growth. Figure 14 shows the growth predicted for a leveling parameter of 1 and a wall angle of 70°. The nonuniformity is the highest of any case treated in this study:  $N_{90} = -29.9\%$ . The associated nonuniformity is plotted as Curve 14 of Figure 15.

### • Moderate leveling, 70° wall angle

**Figure 16** shows growth under the same conditions as above except that  $K_{\text{LEV}}$  was assumed to be 0.5 instead of 1. The degree of nonuniformity,  $N_{90} = -20.5\%$ , is lower than for  $K_{\text{LEV}} = 1$ , but is still among the highest considered. (See Curve 16 in Figure 15.)

### • Mild leveling, 70° wall angle

A still lower value of  $K_{\rm LEV}$ , 0.2, produces yet a milder effect, as shown in **Figure 17**. In that case,  $N_{90} = -10.1\%$ , but the leveling power is still sufficiently strong to cause a full reversal of the "rabbit ears" trend predicted under the same conditions in the absence of leveling  $(K_{\rm LEV} = 0)$ . (See Curve 17 in Figure 15.) Figure 15 compares the nonuniformity-vs.-thickness behavior for four cases with a 70° wall angle. Curves 8, 17, 16, and 14 are for increasing values of  $K_{\rm LEV}$  ranging from 0 to 1. Figures 16 and 17 show some numerical instability toward the end of the growth period, an apparent failure of the numerical method to describe the intense inhibition in

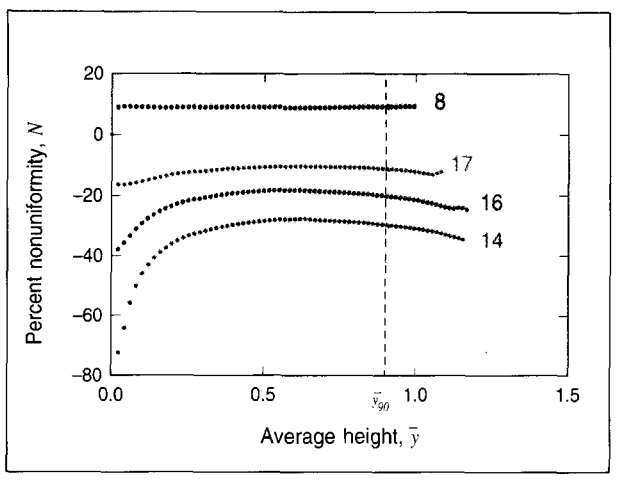


### Figure 15

Predicted relative nonuniformity as a function of the height of the deposited film at a 70° wall angle and four different values of the leveling parameter:  $K_{\rm LEV}=0$  (curve 8);  $K_{\rm LEV}=0.2$  (curve 17);  $K_{\rm LEV}=0.5$  (curve 16);  $K_{\rm LEV}=1$  (curve 14); base conditions otherwise.

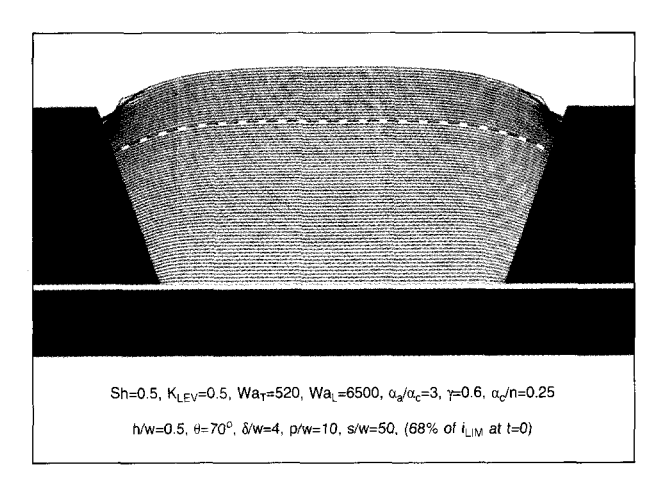


### Figure 16

Shape evolution predicted under moderate leveling and a 70° wall angle ( $K_{\rm LFV} = 0.5$ ,  $\theta = 70^\circ$ , base conditions otherwise).

growth at the walls as the profile advances toward the top of the cavity. The  $N_{90}$  data were determined from shape-history data generated before the onset of this instability.

### • Strong leveling, 110° wall angle

For closed wall angles under leveling, one might expect the opposite of the crowning behavior predicted in the absence of leveling, since leveling acts to reverse the sense

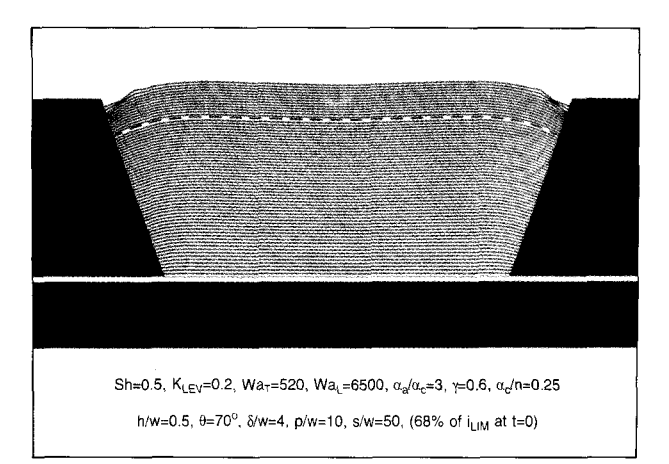


### Figure 17

Shape evolution predicted under mild leveling and a 70° wall angle ( $K_{\rm LEV}=0.2,~\theta=70^\circ$ , base conditions otherwise).

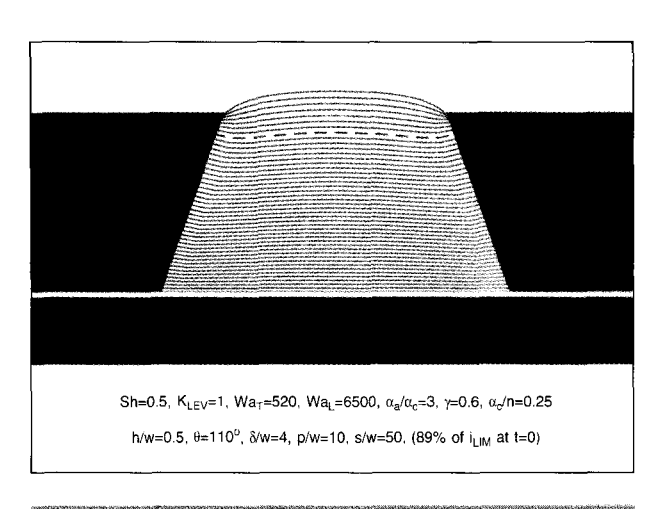


### Figure 18

Shape evolution predicted under strong leveling and a 110° wall angle ( $K_{\rm LEV}=1,~\theta=110^\circ$ , base conditions otherwise).

of the nonuniformity for open wall angles. Interestingly, however, such a reversal is not predicted by the model. Rather, **Figure 18** shows that even strong leveling,  $K_{\rm LEV}=1$ , does not cause the sides to grow higher than the center. The degree of nonuniformity is milder than when no leveling agent is present: In this case,  $N_{90}$  is -3.6% rather than -9.5%. (Ironically, this is the first case for which the term "leveling" seems to apply.) Curve 18 in **Figure 19** shows that the relative nonuniformity, always negative, passes through a minimum in magnitude at approximately 75 percent of the height of the resist and then becomes

strongly negative as the profile becomes increasingly exposed to favorable diffusion toward the mouth of the cavity.

### • Moderate leveling, 110° wall angle

When  $K_{\rm LEV}$  is set to an intermediate value of 0.5 rather than 1 or 0, an intermediate degree of nonuniformity results:  $N_{90} = -5.4\%$  rather than -3.6% or -9.5%. Figure 20 shows the corresponding shape history; the wall angle is again 110°. Again it appears that the impact on  $N_{90}$  is roughly proportional to the value of the leveling parameter over the range investigated. Figure 19 compares three different cases with a 110° wall angle, each with different assumed values of  $K_{\rm LEV}$  ranging from 0 (Curve 10) to 1 (Curve 20). In each case, N is negative throughout; and the leveling action causes a lessening of the nonuniformity due to metal-ion depletion, but does not cause a complete reversal in the sign of N.

### **Conclusions**

Some predictions of a practical nature that are suggested by the analysis are the following:

- At low or moderate fractions of the limiting current, there should be very little tendency for a 10-µm feature created by through-mask electrodeposition without additives to deviate from a flat profile. In order to produce profiles that could be visually recognized as non-flat, it was necessary to choose a high fraction of the limiting current, which would rarely be appropriate in actual fabrication.
- At a high fraction of the limiting current, in the absence of leveling agents, non-flat profiles should result from the uneven transport of metal ions (which causes an uneven overpotential along the feature surface).
  - · When the resist walls are vertical and high, they should guide metal-ion diffusion along parallel lines, which should increase uniformity. However, this collimating effect is expected to be reduced when the resist is thin, and it should gradually vanish as the deposit grows to the height of the resist wall. As this happens, radial or spherical diffusion to the periphery of the feature should gradually become more important, and the result should be dishing or the appearance of "rabbit ears." Accordingly, the rate at which the profile becomes nonuniform should accelerate as the deposit thickness approaches the resist thickness. Another factor that should cause such an acceleration is that the increasingly non-flat profile geometry should cause further nonuniformity in the metal-ion flux. It may therefore be appropriate to use resist layers that exceed the desired thickness of the electrodeposit by an appropriate margin.

- The tendency for the appearance of "rabbit ears" described above should be stronger for a round cavity  $10~\mu m$  in diameter than for a long trench  $10~\mu m$  in width. This is because the spherical enhancement in axisymmetric geometries is predicted to be stronger than the radial enhancement in two-dimensional geometries.
- When the resist wall makes an obtuse angle with the feature surface ( $\theta > 90^{\circ}$ ), there should be a tendency from the beginning toward geometrically enhanced diffusion to the periphery, and the formation of "rabbit ears."
- When the resist wall makes an acute angle with the feature surface ( $\theta < 90^{\circ}$ ), there should be a steady tendency toward higher depletion of metal ions at the periphery, which should lead to crowning.
- The analysis predicts that in the presence of agents which act in accordance with the diffusion theory of leveling, the natural tendency for flat microprofiles seen in nonleveling systems can be upset. This is so chiefly because a resist-patterned surface is highly nonuniform from the standpoint of accessibility to the electroactive portions by diffusing species. Leveling agents, which operate at their diffusion-limited fluxes, are very sensitive to such nonuniformities. (Although the metal ions are similarly sensitive, they are normally far from their diffusion limits and exert little effect.)
  - As a general rule, strong leveling should cause relatively slower growth in regions affected by geometrically enhanced diffusion, and growth should be faster in those regions to which diffusion is geometrically disfavored. Hence, structures that produced rabbit ears in nonleveling baths at high current density should generally produce crowning under strong leveling. One could reason that the inverse trend should also apply: In systems where metal-ion completion produces a crowned deposit, strong leveling should produce rabbit ears. Such a complete reversal was not illustrated in the present study, but Figure 19 clearly shows that the degree of crowning should be decreased by leveling. Perhaps a complete reversal was not seen because the assumed fraction of limiting current was so high for the 110°-wall-angle cases that metal-ion depletion outweighed the leveling effect.

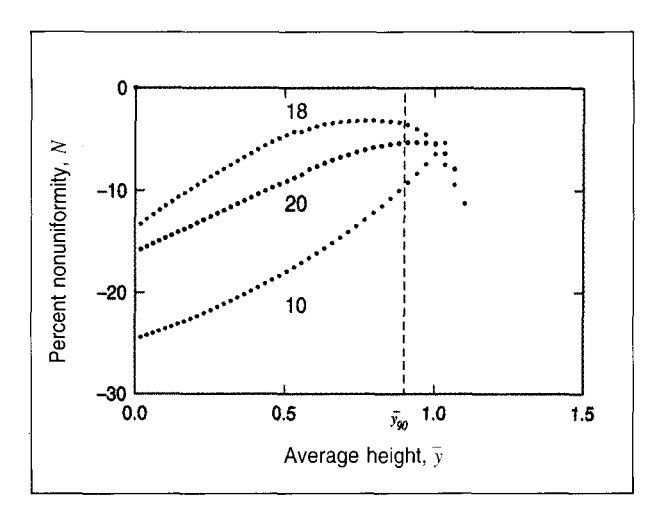
### List of symbols and base values of parameters

• Variables (dimensional)

 $\begin{array}{ll} \phi & \text{potential within the electrolyte (V)} \\ c_{\text{M}} & \text{concentration of the depositing metal ion (mol/cm}^3) \end{array}$ 

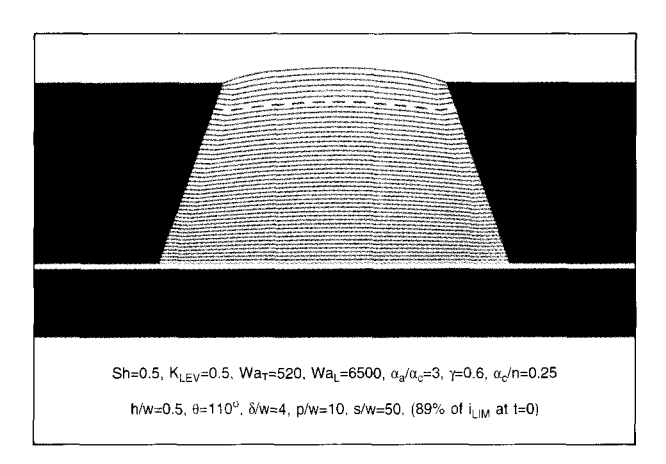
 $c_{\rm A}$  concentration of the leveling agent (mol/cm<sup>3</sup>)

i current density at the cathode surface (mA/cm<sup>2</sup>)



### Elminia (F.)

Predicted relative nonuniformity as a function of the height of the deposited film at a 110° wall angle and three different values of the leveling parameter:  $K_{\rm LEV}=0$  (curve 10);  $K_{\rm LEV}=0.5$  (curve 20);  $K_{\rm LEV}=1$  (curve 18); base conditions otherwise.



### G attracks

Shape evolution predicted under moderate leveling and a 110° wall angle ( $K_{\rm LEV}=0.5,~\theta=110^\circ$ , base conditions otherwise).

 $N_{\rm M}$  flux of metal ion at the cathode surface (mol/cm<sup>2</sup>-s)  $N_{\rm A}$  flux of leveling agent at the cathode surface (mol/cm<sup>2</sup>-s)

### • Geometric and operating parameters

	1 01	
Symbol	Meaning	Base value
w	initial width of base of cavity	10 μm
h	height of resist wall	5 μm
$\theta$	resist wall angle	90°
p	pitch (intercavity spacing)	$100 \mu m$

S	height of constant-i plane	1 cm	117
ī	average initial current density to feature	50 mA/cm <sup>2</sup>	$Wa_{_{\mathrm{T}}}$
$c_{M}^{\infty}$	bulk concentration of metal ion	100 mM	$\frac{\alpha_{\rm a}}{}$
$c_A^{\infty}$	bulk concentration of leveling agent	0 mM	$\alpha_{_{ m c}}$
δ	thickness of diffusion boundary layer	$40 \mu m$	
T	absolute temperature	298 K	$Wa_{_{ m L}}$

### • Physico-chemical constants

Symbol	Meaning	Base value
κ	electrolyte conductivity	$0.5~\Omega^{-1}~cm^{-1}$
$i_{0, c_{\mathbf{A}}=0}^{\infty}$	exchange current density at $c_{\rm M} = c_{\rm M}^{\infty}$ and $c_{\rm A}^{\infty} = 0$	1 mA/cm <sup>2</sup>
$\alpha_{\rm a}, \alpha_{\rm c}$	transfer coefficients	1.5, 0.5
n	number of electrons transferred	2
γ	exponent in $i_0$ - $c_{\rm M}$ relation	0.6
R	universal gas constant	8.314 J/mol-K
$\boldsymbol{F}$	Faraday's constant	96 487 coulombs
$k_{ m LEV}$	constant in inhibition model	0
$D_{M}$	metal-ion diffusivity	$5.2 \times 10^{-6} \text{ cm}^2/\text{s}$
$D_{A}$	leveling-agent diffusivity	

### • Dimensionless variables

Symbol	Expression	Meaning
$\phi^*$	$\frac{\phi \kappa}{\bar{i} w}$	dimensionless potential
$c_{\scriptscriptstyle \mathrm{M}}^*$	$rac{c_{_{ m M}}}{c_{_{ m M}}^{^{\infty}}}$	dimensionless metal-ion concentration
$c_{\rm A}^*$	$rac{c_{_{ m A}}}{c_{_{ m A}}^{^{\infty}}}$	dimensionless leveling-agent concentratio
i*	$\frac{i}{\overline{i}}$	dimensionless current density
$N_{\scriptscriptstyle m M}^*$	$\frac{N_{\rm M}w}{D_{\rm M}c_{\rm M}^{\infty}}$	dimensionless metal-ion flux
$N_{\scriptscriptstyle  m A}^*$	$\frac{N_{\rm A}w}{D_{\rm A}c_{\rm A}^{\infty}}$	dimensionless leveling-agent flux

### • Seven dimensionless parameters

Symbol	Expression	Name	Base value
Sh	$\frac{\overline{i}w}{nFD_{\rm M}c_{\rm M}^{\infty}}$	Sherwood number	0.5
γ		(exponent in kinetic expression)	0.6
$K_{\mathrm{LEV}}$	$\frac{nFc_{A}^{*}D_{A}}{\overline{i}w}k_{LEV}$	normalized leveling parameter	0
$\frac{\alpha_{\rm c}}{\alpha_{\rm c}}$		(ratio of $\alpha_c$ to $n$ )	0.25

$Wa_{_{\mathrm{T}}}$	$\frac{RT\kappa}{\alpha_c F \bar{i} w}$	Wagner number, Tafel form	520
$\frac{\alpha_{\rm a}}{\alpha_{\rm c}}$		(ratio of transfer coefficients)	3
$\mathit{Wa}_{\scriptscriptstyle  m L}$	$\frac{RT\kappa}{(\alpha_{\rm c} + \alpha_{\rm a})Fi_{0, c_{\rm A}=0}^{\infty}w}$	Wagner number, linear form	6500

### Other symbols

diameter of no-flux cylinder surrounding a round cavity (cm)
average initial limiting current density to feature $(mA/cm^2)$
current density at boundary far away from cathode $(mA/cm^2)$
unit vector normal to surface (cm)
current density in presence of leveling agent (mA/cm²)
current density in absence of leveling agent (mA/cm²)
normalized height nonuniformity (dimensionless)
value of N when $\bar{y}$ is 90 percent of resist height
average height of deposited film
height of profile at center of feature
height of profile at opposite extreme from center
surface overpotential (V)
concentration overpotential (V)
total overpotential (V)

### **Acknowledgments**

The author is grateful to L. T. Romankiw, S. Mehdizadeh, P. C. Andricacos, M. R. Kordus, Anantharaman V., and Professor S. S. Kruglikov for helpful discussions; and to Anantharaman V. for proofreading the manuscript.

### References

- L. T. Romankiw, "Thin Film Inductive Heads: From One to Thirty One Turns," Proceedings of the Symposium on Magnetic Materials, Processes, and Devices, L. T. Romankiw and D. A. Herman, Jr., Eds., The Electrochemical Society, Inc., Pennington, NJ, 1990, Vol. 90-8, pp. 39-53.
- R. E. Acosta, "Fabrication of Masks for Synchrotron X-Ray Lithography," Proceedings of the Symposium on Electrochemical Technology in Electronics, L. T. Romankiw and T. Osaka, Eds., The Electrochemical Society, Inc., Pennington, NJ, 1988, Vol. 88-23, pp. 257-262.
- S. Krongelb, J. O. Dukovic, M. L. Komsa, S. Mehdizadeh, L. T. Romankiw, P. C. Andricacos, A. T. Pfeiffer, and K. Wong, "The Application of Electrodeposition Processes to Advanced Package Fabrication," Proceedings of the SPIE International Conference on Advances in Interconnection and Packaging, 1990, Vol. 1389, pp. 249-256.

- C. G. Woychik and R. C. Senger, "Joining Materials and Processes in Electronic Packaging," *Principles of Electronic Packaging*, D. P. Seraphim, R. Lasky, and C. Y. Li, Eds., McGraw-Hill Book Co., Inc., New York, 1989, pp. 595–598.
- L. C. Matthew, P. W. Coteus, A. P. Lanzetta, and W. P. Pawlowski, "Flex Fabrication—Practical Problems and Design Considerations," S. Khadpe, Ed., Proceedings of the Fourth International TAB Symposium, San Jose, February 16-19, 1992, Semiconductor Technology Center, Neffs, PA, 1992, pp. 173-182.
- R. R. Tummala, R. W. Keyes, W. D. Grobman, and S. Kapur, "Thin-Film Packaging," *Microelectronics Packaging Handbook*, R. R. Tummala and E. J. Rymaszewski, Eds., Van Nostrand Reinhold, New York, 1989, pp. 673-725.
- L. T. Romankiw and T. A. Palumbo, "Electrodeposition in the Electronic Industry," Proceedings of the Symposium on Electrodeposition Technology, Theory and Practice, L. T. Romankiw and D. R. Turner, Eds., The Electrochemical Society, Inc., Pennington, NJ, 1987, Vol. 87-17, pp. 13-41.
- L. T. Romankiw, S. Krongelb, E. E. Castellani, J. Powers, A. Pfeiffer, and B. Stoeber, "Additive Electroplating Technique for Fabrication of Magnetic Devices," *Proceedings of the International Conference on Magnetics, ICM-73*, 1973, Vol. 6, pp. 104-111.
   E. C. Hume III, W. M. Deen, and R. A. Brown, "Mass
- E. C. Hume III, W. M. Deen, and R. A. Brown, "Mass Transfer Analysis of Electrodeposition Through Polymeric Masks," *J. Electrochem. Soc.* 131, No. 6, 1251–1258 (1984).
- J. O. Dukovic, "Computation of Current Distribution in Electrodeposition, a Review," *IBM J. Res. Develop.* 34, No. 5, 693-705 (1990).
- J. O. Dukovic and C. W. Tobias, "Simulation of Leveling in Electrodeposition," *J. Electrochem. Soc.* 137, No. 12, 3748–3755 (1990).
- J. Newman, Electrochemical Systems, Prentice-Hall, Inc., Englewood Cliffs, NJ, 1991, pp. 196–197.
- 13. Ibid., p. 433.
- O. Kardos and D. G. Foulke, "Applications of Mass Transfer Theory: Electrodeposition on Small-Scale Profiles," Adv. Electrochem. & Electrochem. Eng. 2, 145-233 (1962).
- O. Kardos, "Leveling and Microthrowing Power," Galvanotechnik und Oberflachenschutz 8, 161, 185 (1967) (also in Proceedings of Surface 66, Basel, 1966, pp. 62-72).
- S. S. Kruglikov, N. T. Kudryavtsev, G. I. Medvedev, and T. M. Izmailova, "A Study of Levelling in Nickel and Copper Plating Solutions," Trans. Inst. Metal Finish. 42 (1964); Proceedings of the 6th International Conference on Electrodeposition and Metal Finishing, London, 1964, pp. 129-137.
- N. Ibl, "Diffusion Layers—Influence of Mass Transport on the Structure of Electrolytic Deposits," Galvanotechnik und Oberflachenschutz 7, 256 (1966) (also in Proceedings of Surface 66, Basel, 1966, pp. 48-61).
- S. S. Kruglikov, N. T. Kudryavtsev, G. F. Vorobiova, and A. Ya. Antonov, "On the Mechanism of Levelling by Addition of Agents in Electrodeposition of Metals," *Electrochim. Acta* 10, 253–261 (1965).
- K. G. Jordan and C. W. Tobias, "The Effect of Inhibitor Transport on Leveling in Electrodeposition," J. Electrochem. Soc. 138, No. 5, 1251-1259 (1991).
- S. I. Krichmar, "Theory of the Leveling Effect in the Electrochemical Behavior of Metals," Sov. Electrochem.
   No. 7, 763-766 (1965) (translated from Elektrokhimiya 1, No. 7, 858-861 (1965).
- D. Roha and U. Landau, "Abstract No. 571: A Transport Based Theory for Leveling Additives," *Electrochemical*

- Society Extended Abstracts, The Electrochemical Society, Inc., Pennington, NJ, 1987, Vol. 87-2, pp. 803-804.
- D. Roha and U. Landau, "Abstract No. 326: Non-Steady State Modeling of Transport Controlled Plating Additives," *Electrochemical Society Extended Abstracts*, The Electrochemical Society, Inc., Pennington, NJ, 1988, Vol. 88-2, pp. 477-478.
- 23. C. A. Brebbia and S. Walker, *Boundary Element Techniques in Engineering*, Newnes-Butterworths, Boston, 1980
- J. Dukovic and C. W. Tobias, "The Influence of Attached Bubbles on Potential Drop and Current Distribution at Gas-Evolving Electrodes," J. Electrochem. Soc. 134, No. 2, 331-343 (1987).

Received March 12, 1992; accepted for publication November 9, 1992

John O. Dukovic IBM Research Division, Thomas J. Watson Research Center, P.O. Box 218, Yorktown Heights, New York 10598 (DUKOVIC at YKTVMV, dukovic@watson.ibm.com). Dr. Dukovic received his B.S. degree in chemical engineering from Case Western Reserve University, Cleveland, Ohio, in 1980, and his Ph.D. in chemical engineering from the University of California at Berkeley in 1986. His current activities as a Research Staff Member at the IBM Thomas J. Watson Research Center include the electrodeposition of packaging and wiring structures, process control, and electrodeposition process modeling. Dr. Dukovic is an Adjunct Assistant Professor of Chemical Engineering and Applied Chemistry at Columbia University. He is a member of the American Electroplaters and Surface Finishers Society, the American Institute of Chemical Engineers, and the Electrochemical Society.

